Voltage-Dependent Insertion of Alamethicin at Phospholipid/Water and Octane/Water Interfaces

D. P. Tieleman,* H. J. C. Berendsen,† and M. S. P. Sansom*

*Laboratory of Molecular Biophysics, Department of Biochemistry, University of Oxford, The Rex Richards Building, South Parks Road, Oxford OX1 3QU, United Kingdom; †Dept. of Biophysical Chemistry, University of Groningen, Nijenborgh 4, 9747 AG Groningen, The Netherlands

ABSTRACT Understanding the binding and insertion of peptides in lipid bilayers is a prerequisite for understanding phenomena such as antimicrobial activity and membrane-protein folding. We describe molecular dynamics simulations of the antimicrobial peptide alamethicin in lipid/water and octane/water environments, taking into account an external electric field to mimic the membrane potential. At *cis*-positive potentials, alamethicin does not insert into a phospholipid bilayer in 10 ns of simulation, due to the slow dynamics of the peptide and lipids. However, in octane N-terminal insertion occurs at field strengths from 0.33 V/nm and higher, in simulations of up to 100 ns duration. Insertion of alamethicin occurs in two steps, corresponding to desolvation of the Gln7 side chain, and the backbone of Aib10 and Gly11. The proline induced helix kink angle does not change significantly during insertion. Polyalanine and alamethicin form stable helices both when inserted in octane and at the water/octane interface, where they partition in the same location. In water, both polyalanine and alamethicin partially unfold in multiple simulations. We present a detailed analysis of the insertion of alamethicin into the octane slab and the influence of the external field on the peptide structure. Our findings give new insight into the mechanism of channel formation by alamethicin and the structure and dynamics of membrane-associated helices.

INTRODUCTION

The interactions between polypeptides and membranes are of fundamental importance for a variety of cellular processes, including membrane protein folding and the action of toxins and antimicrobial peptides (White and Wimley, 1999; Epand and Vogel, 1999). In many processes the membrane potential plays a crucial role in the function of membrane proteins. Examples are voltage-gated ion channels, signaling, transduction by sensory receptors, and cellular mobility (Stryer, 1988). The action of certain antimicrobial peptides can also depend critically on a transmembrane voltage difference (Sansom, 1991).

Recently, there has been considerable progress in studies of peptides bound to bilayers. Traditionally this is a difficult area for structural studies because neither crystallography nor solution nuclear magnetic resonance spectroscopy (NMR) is well suited for this type of system. However, several techniques including X-ray diffraction (Hristova et al., 1999), solid state NMR (Bechinger, 1999; Kovacs et al., 2000; Marassi and Opella, 1998), Fourier transform infrared spectroscopy (FTIR; Arkin et al., 1995; Goormaghtigh et al., 1999), amide hydrogen-deuterium exchange NMR measurements (Halsall and Dempsey, 1999) and circular dichroism spectroscopy (CD) combined with isothermal titration calorimetry (Wieprecht et al., 1999) have allowed glimpses of the structure and orientation of several amphipathic helices and other peptides bound to or inserted in phospholipid bilayers. In addition, peptide synthesis has allowed systematic variation of the sequence of model peptides to study the determinants of peptide structure near a phospholipid bilayer (Bechinger, 1996; Lu and Deber, 1998) and of peptide aggregation behavior in a lipid environment (Zhou et al., 2000; Choma et al., 2000).

Several peptides form voltage-activated channels with well-defined conductance levels (Sansom, 1991). Because these channels are relatively simple, they form attractive model systems for understanding lipid-peptide interactions, aggregation behavior, and ion channel properties. One of the best studied channel-forming peptides is alamethicin (Alm), a member of the family of peptaibols. Its pore-forming and structural properties have been extensively reviewed (Woolley and Wallace, 1992; Sansom, 1993; Cafiso, 1994), and a large number of recent studies on binding and insertion interactions with lipid bilayers are available, both experimental (North et al., 1995; He et al., 1996; Dempsey and Handcock, 1996; Barranger-Mathys and Cafiso, 1996; Lewis and Cafiso, 1999) and computational (Biggin et al., 1997; Tieleman et al., 1999b,c; Kessel et al., 2000).

Alm occurs in two native forms, the R_f30 form:

Ac-Aib-Pro-Aib-Ala-Aib-Ala-Gln-Aib-Val-Aib-

Gly-Leu-Aib-Pro-Val-Aib-Aib-Glu-Gln-Phl

and the R_f50 form, in which the Glu at position 18 is replaced by a Gln, making the peptide electrically neutral. Alm contains a central Gly-X-X-Pro motif, which forms a molecular hinge between the two predominantly α-helical

Received for publication 16 June 2000 and in final form 28 September 2000.

Address reprint requests to D. P. Tieleman, Department of Biological Sciences, University of Calgary, 2500 University Drive NW, Calgary, Alberta T2N 1N4, Canada. Fax: 403-289-9311; E-mail: tieleman@ucalgary.ca.

© 2001 by the Biophysical Society

0006-3495/01/01/331/16 $2.00

segments (Fox and Richards, 1982; Esposito et al., 1987; Franklin et al., 1994) and is rich in the helix-promoting residue α-aminoisobutyric acid (Aib). The C-terminal residue is a phenylalanine with the carboxy terminus replaced by a hydroxyl group (phenylalaninol). The structure of Alm is shown in Fig. 1.

Channel activation by Alm is strongly voltage-dependent. It has been suggested that the voltage-dependent step of channel formation is a voltage-induced insertion of Alm into the bilayer and/or a change in conformation of the peptide (Fox and Richards, 1982; Woolley and Wallace, 1992; Sansom, 1993; Cafiso, 1994). Alm binds to the surface of a lipid bilayer, but can also insert into a bilayer, depending on the type of lipid, temperature, hydration level and peptide concentration (Vogel, 1987; Huang and Wu, 1991; North et al., 1995; He et al., 1996; Dempsey and Handcock, 1996; Jayasinghe et al., 1998). Figure 1 sketches the main proposed steps in channel formation.

Computer simulations of atomistic models can provide detailed information on the structure of proteins and peptides in the membrane environment and on binding and insertion processes (Tieleman et al., 1997). Currently simulations of hundreds of nanoseconds are feasible on relatively simple systems. Such simulations have been used to obtain insight into the folding of a small protein (Duan and Kollman, 1998) and into the reversible folding of peptides, allowing unprecedented comparison with and interpretation of NMR data on the same system (Daura et al., 1998, 1999). Simulations have also provided insight into the folding and partitioning of poly-leucine and a simple amphipathic peptide at the interface between water and hexane (Chipot and Pohorille, 1998; Chipot et al., 1999). Simulations of peptides bound to phospholipid bilayers have proved to be more difficult, due to the long time scales of lipid relaxation and peptide motion compared to typical current simulation lengths of the order of 0.5 to 4 ns. Nonetheless, there have been several recent studies of melittin (Bernèche et al., 1998; Bachar and Becker, 2000), dermaseptin (La Rocca et al., 1999), and alamethicin (Tieleman et al., 1999b). The high level of detail in such simulations holds great promise for obtaining a detailed understanding of lipid-peptide interactions.

Here we extend the work of Biggin et al. (1997), who used molecular dynamics simulations in a hydrophobic potential representing the membrane; and a previous study in which we simulated Alm bound to a palmitoyl-oleoyl-phosphatidylcholine (POPC) bilayer and in water (Tieleman et al., 1999b). The current model includes water, a phospholipid bilayer, or octane, and an approximate description of the transmembrane potential. Our aim is to understand the voltage-dependent insertion of Alm at an atomic level. Specific questions include: what are the conformational changes in Alm upon insertion; what are the energetics of the process of insertion; and what is the origin of the voltage dependency of channel formation by Alm? We compare simulations of Alm with control simulations of an ideal poly-alanine helix in order to distinguish general properties of hydrophobic α-helices from features specific to Alm.

These questions may be of broader interest with respect to peptides and proteins other than alamethicin. Alamethicin can be viewed as a simple and well-characterized model system for channel forming peptides, but also as a model system for more complex ion channels formed by parallel helices, ranging from the ~100-residue Influenza A M2 peptide (Kukol et al., 1999) to complex gated channels such as the nicotinic acetylcholine receptors (Miyazawa et al., 1999) and the mechano-sensitive channel MscL (Chang et al., 1998). Indeed, the behavior of simple transmembrane helices may be relevant for a wide range of complex membrane proteins. In addition, simple peptides are useful tools to study the thermodynamics of lipid-peptide interaction and peptide folding (White and Wimley, 1998, 1999; Daura et al., 1998), a field in which we expect molecular simulations to contribute significantly.

In this study, we describe the structure and stability of Alm in the different environments and the voltage-driven insertion of Alm into the octane slab. We performed a number of simulations of alamethicin in a phospholipid bilayer, in water, and in octane, at different electrostatic

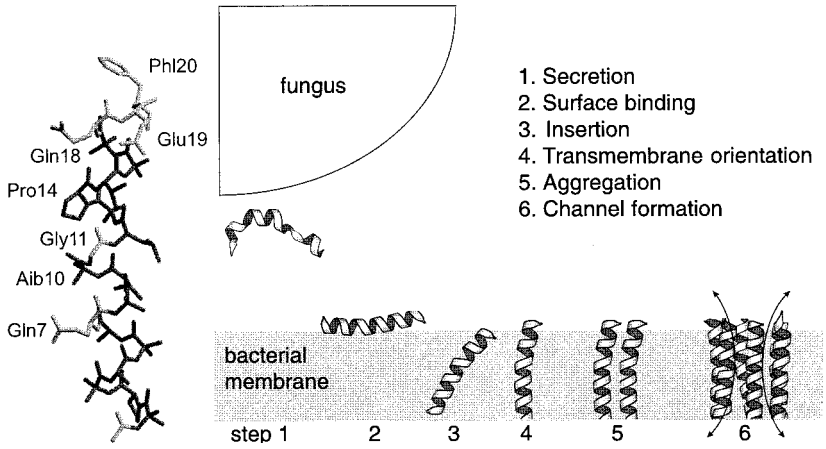

FIGURE 1 (*A*) Structure of alamethicin. Highlighted are the hydrophilic residues at the C-terminus (Phl20, Gln19, Glu18), the key residues Gln7, Aib10, Gly11, and Pro14. (*B*) Hypothetical idealized mechanism of channel formation of alamethicin. Secreted Alm molecules undergo a conformational change towards helix at the membrane. Steps 3–5 are hypothetical (see Discussion). The last step is channel formation. At least one step in the mechanism is voltage-dependent.

fields, and in surface bound, i.e., parallel to the water/lipid or water/octane interface, and inserted, i.e., perpendicular to the water/lipid or water/octane interface, orientations. As control simulations we also simulated a polyalanine helix in different environments, pure water and water/octane at different electrostatic field strengths. Table 1 lists the most important simulations and Fig. 2 shows the different systems, the box dimensions, and the direction of the applied electric field.

METHODS

Setup of the simulation systems

Alamethicin/POPC

The simulation protocol and starting structure for the Alm-POPC systems are the same as in a previous study of Alm (Tieleman et al., 1999b). For Alm/POPC (see Table 1) the sodium ion in the original system was simply deleted. Alm-/POPC and Alm-/POPC/0.66 contain 128 POPC lipids, 3552 water molecules, and 1 sodium ion; Alm/POPC contains 128 POPC lipids and 3552 water molecules. The total number of atoms in all three systems is 17,480. The initial area of the water/lipid interface is 36.7 nm^2. The area in all three simulations did not change appreciably and was still 36.6–36.7 nm^2 after 10 ns. Lipid parameters were taken from Berger et al. (1997) and for the double bond in the lipid from GROMOS87, the peptide used a slightly modified GROMOS87 parameter set, and SPC was used as water model (Berendsen et al., 1984). Simulations were run with a 2-fs timestep, a 1.0/1.7 nm group-based twin range cutoff for electrostatic interactions, without switch or shift function. The neighbor list was updated every 10 steps. The pressure, independently in *x*, *y*, and *z* at 1.0 bar ($\tau_p = 1.0$ ps), and temperature (300 K, $\tau_T = 0.1$ ps, protein, lipid, and water separately) were controlled with the weak coupling method (Berendsen et al., 1981).

Alamethicin/octane and poly-alanine/octane

Pre-equilibrated water and octane systems were made at 300 K with a lateral size of 4 × 4 nm. The two systems were merged and simulated for a nanosecond with constant *x* and *y*, whereas the pressure was allowed to fluctuate in the *z* dimension. An Alm peptide model used in previous work (Tieleman et al., 1999b) was oriented with its helical axis parallel to the interface, with its hydrophilic face towards water, and located as close as possible to the octane slab without overlap between the peptide and octane atoms. Water was removed within van der Waals distance from the peptide. This system was minimized and used as starting structure for all simulations that started with Alm on the interface. Note that neither distance nor orientation of the peptide at the water/octane system is critical, since the peptide reorients within a few hundred picoseconds, in sharp contrast to the situation in a phospholipid interface.

For poly-alanine simulations starting structures were created by best fitting an ideal 20-residue polyalanine, with Ace and NH2 caps, helix on the Alm peptide and energy minimizing the system. As starting structure for the runs with the peptide inserted in octane, a structure from the Alm/0.67 simulation (Table 1) after 3.5 ns was taken. At this point, Alm is already spanning the octane phase. The starting Alm and Ala structures were best fit on the slightly distorted Alm structure in the configuration after 3.5 ns and the system was energy-minimized before production runs. All Alm and Ala systems in octane contain 182 octane molecules and 1618 water molecules (total for Alm, 6478 atoms; for Ala, 6436 atoms).

Alm/water and Ala/water were created in the usual way, stacking a pre-equilibrated water system to form a cubic box big enough to contain the peptides, removing water molecules that overlap with peptide atoms, and minimizing energy. This resulted in a cubic box of 4.9 nm^3 with 3841 water molecules for poly-alanine (total: 11,648 atoms) and a box of 4.9 nm^3 with 3789 water molecules (total: 11,535 atoms).

For the Alm-octane systems we used the GROMOS96 43a2 force field (van Gunsteren et al., 1996; Schuler and van Gunsteren, 2000) as implemented in GROMACS (van der Spoel et al., 1998; Berendsen et al., 1995). SPC was used as water model. A group-based twin-range cutoff of 0.8/1.4 nm, without shift or switch functions, was used for both Coulomb and Lennard Jones interactions. This is probably acceptable, considering the peptides are not charged. Alternative methods like reaction field corrections or Ewald summation are less appropriate for the inhomogeneous systems with areas with low dielectric constant (Hunenberger and McCammon, 1999), although currently detailed knowledge of the precise effect of different electrostatic approximations in membrane systems is lacking. The timestep was 5 fs, using hydrogen atoms with an increased mass of 4 atomic mass units (amu) and a special treatment of hydrogens and the Phl aromatic ring (Feenstra et al., 1999). Briefly, this entails calculating the forces on the hydrogens, but instead of updating the positions of the hydrogens with these forces, the forces are redistributed over neighboring heavy atoms, and the position of the hydrogen is reconstructed every step, assuming an ideal geometry. This effectively removes the degrees of freedom involving the hydrogen atoms while still generating correct forces and pressure for the system as a whole. For the positions of the carbons in the aromatic ring, which is a construct of improper dihedrals, a similar

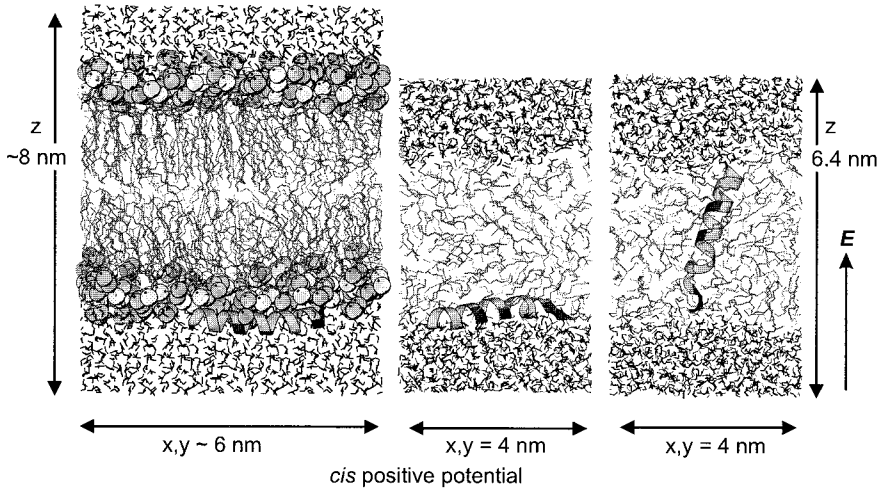

FIGURE 2 Overview of the three main simulation systems, with the dimensions and direction of the applied electrical field. (*left*) Starting structure of Alm/POPC simulation. (*middle*) Snapshot of a surface-bound Alm in octane. (*right*) Snapshot of an inserted Alm. The poly-alanine systems have the same dimensions.

TABLE 1 Overview of the peptide simulations featured in this work

System name	Length	System name	Length
Lipid bilayer		Negative field	
Alm-/POPC/0.66	10 ns	Alm/−0.33	5 ns
Alm-/POPC	10 ns	Alm/−0.67	2 ns
Alm/POPC/0.66	10 ns	Alm/−1.0	2 ns
Alm in octane		Ala in octane	
Alm/0.0	50 ns	Ala/0.0	10 ns
Alm/0.1	100 ns	Ala/0.33	20 ns
Alm/0.33	35 ns	Ala/0.67	5 ns
Alm/0.50	15 ns	Ala/1.0	2 ns
Alm/0.67	5 ns	Ala/0.0-ins	10 ns
Alm/1.0	2 ns	Ala/0.1-ins	10 ns
Alm/0.0-ins	20 ns		
Alm/0.1-ins	20 ns		
Alm and Ala in water			
Alm/SOLa	2.5 ns	Alm/SOLc	2.5 ns
Alm/SOLb	2.5 ns	Ala/SOL	2.5 ns

The names of the simulations indicate whether POPC, octane, or water was used, the strength of the external electrostatic field (in V/nm) in the simulation (a positive field means in the direction indicated in Fig. 2), and, for the POPC simulations, whether Glu19 was charged or not. For all other simulations Glu19 was protonated. 'ins' means the peptide started inserted in an octane slab. For each run the length of the simulation is given. Fields of 2 V/nm cause breakdown of the octane/water interface, and simulations at this strength have not been analyzed in detail.

method is used. The neighbor list was updated every 3 steps. Bond lengths were constrained with LINCS (Hess et al., 1997). Water, protein, and octane were coupled separately to a temperature bath at 300 K with τ_T = 0.1 ps. The surface area of the system was fixed, but the pressure in the *z* direction was kept at 1 bar using weak pressure coupling (Berendsen et al., 1984), with τ_p = 1.0 ps. The titratable residue Glu18 was assumed to be in its neutral form. Although this is a matter of debate, in this work it should not matter much. The Alm version with Gln18 (instead of Glu18) behaves similarly for our purpose. If Glu18 inserts in the octane phase, it is likely to be protonated. If it is solvent exposed at the hydrophilic C-terminus, we underestimate the strength of water-Glu18 interactions, which, however, are already strong.

Polyalanine and Alm were simulated with the same parameters in water, using isotropic pressure scaling. We repeated the same 2.5-ns simulation from different starting velocities three times for Alm, twice with a 2-fs timestep and once with a 5-fs timestep and dummy constructs for hydrogens and Phl (see above).

To test the effect of an external electric field on water structure and total potential, we ran five simulations of pure water at applied fields of 0, 0.1, 0.33, 1.0, and 10 V/nm, plus one simulation at 0.1 V/nm with a larger time step. In addition, we simulated the basic water/octane system used in the peptide simulations with and without external field of 1.0 V/nm for 3 ns.

Application of an external field

In cells, the transmembrane potential difference arises from a difference in concentrations of ions within and outside the cell and in relative permeability K^+ vs. Na^+ ions of the cell membrane. In experiments, a potential difference can be imposed by means of a voltage clamp to maintain a fixed potential difference ΔV. In a system with an impermeable flat membrane of thickness *d* and in the presence of electrolyte, this will result in a nearly constant field of $\Delta V/d$, with *d* the membrane thickness, across the membrane and effectively zero field in the bulk solution (Hille, 1992).

In simulation systems with a box size of the order of nanometers, the subtle imbalance in ionic concentration causing a transmembrane potential of a few hundred mV is impossible to obtain by adding explicit ions to the solution (Roux, 1997). Even if the system would be one or two orders of magnitude larger, which would allow a suitable concentration difference, there still is the problem that there is no real inside and outside of the membrane in simulations that use periodic boundaries. Roux (1997) has described an extension of the work of Ben-Tal et al. (1996) and Ben-Shaul et al. (1996), based on continuum electrostatics theory, to calculate the effect of the transmembrane potential effect on the free energy of membrane proteins. However, this approach relies on the assumptions of continuum electrostatics (i.e., solvent and membrane are dielectric constants without atomic properties), which is difficult to combine with atomistic simulations. Therefore, we used a simple approximation.

In a water/membrane/water system with an impermeable membrane and no electrolyte, the potential is given by the boundary conditions and Poisson's equation. Assuming the potential is 0 V at one end of the box, ignoring periodic boundaries, and *x* V at the other end, the resulting electrostatic problem is simple: the field in each of the three regions is constant and proportional to $1/\epsilon$, with ϵ the local dielectric constant. For water this is 80 (about 60 for the SPC model; Smith and van Gunsteren, 1994; for octane this is 2 (1 in the simulation). Water polarizes linearly with the field up to external applied field strengths of about 1 V/nm (data from the water control simulations, details not shown), so that the linear dielectric approximation is applicable. By adding a term $F_i = q_iE$ with *E* a constant field to the forces on all atoms *i*, the local field at any point will be the sum of this applied field plus the field caused by the orientation of the water molecules, roughly E/ϵ, in our geometry E_z/ϵ. Therefore, the total field in the water phase will be very small, but the total field in the octane phase is practically the same as the externally applied field. This treatment is inconsistent with periodic boundary conditions, because the potential is discontinuous at the box edge. However, this inconsistency affects only the electrostatic energy, not the dynamics, and is therefore expected to be insignificant in our simulations. In the two Alm-/POPC simulations the sodium ion acquires a systematic velocity due to the external field until it resides somewhere in the lipid interface and does not significantly move after an initial 500 ps of simulation. It plays no role in the rest of this study. In the octane systems no ions are present.

The applied external field is rather high. We focused on the Alm/0.33 simulation, because it is the simulation in which insertion occurs at the lowest transmembrane voltage, about 1 V. This is 4 to 6 times as high as a physiological transmembrane voltage. However, the insertion process at 0.50 V/nm looks very similar to that at 0.33 V/nm, which leads us to believe that it will also be similar at lower field strengths. Further development and testing of methods to include the physiological transmembrane potential in molecular dynamics simulations is needed.

There are several logical extensions to this kind of approximation of the transmembrane potential difference. The effect of electrolyte can be taken into account by applying a field derived from a solution of the Poisson-Boltzmann equation or a field derived from a large and computationally expensive simulation of an explicit salt solution at an interface. In a similar fashion, the effect of headgroup and carbonyl group charges of the lipids could be approximately incorporated. Finally, a more rigorous and complex approach will be the incorporation of a simulation system in atomic detail within a larger (infinite) system described by continuum electrodynamics equations with appropriate boundary conditions consistent with the presence of electrodes or an asymmetric salt solution.

Summarizing, we apply a constant external field to all charged atoms. This field acts in full on charges in the octane phase (the peptide), but only to a negligible extent on charges in the water phase because of the polarization of water under the influence of the external field. In the range of applied field strengths used in the main simulations in this study, water responds like a linear dielectric. We do not try to mimic the complex charge distribution of a phospholipid bilayer in the simulations with octane.

The use of octane as membrane mimetic

In a sense, the use of an octane/water interface as model system for a membrane falls between simulations of a lipid bilayer in full atomic detail and continuum electrostatics calculations on membrane proteins that typically use a representation of a membrane consisting of three distinct dielectric regions, corresponding to the low dielectric membrane interior and two high dielectric regions outside the membrane (Ben-Tal and Honig, 1996; Kessel et al., 2000). The main advantage of continuum solvation models is their ability to yield free energies at a moderate computational cost. However, the representation of the membrane is greatly simplified, and, so far, such calculations lack molecular flexibility and dynamics. It is possible to sample peptide configurations in a continuum solvation model (La Rocca et al., 1999), but to combine molecular dynamics with such a model would require a sophisticated treatment of friction in different regions of the bilayer. This would be very useful, and simulations such as we present here can be used to derive appropriate friction coefficients. The main advantages of simulations with octane as membrane mimetic are (i) they include all structural and dynamic details of the peptide, (ii) they include a decent representation of water and the hydrophobic membrane interior and are expected to be an accurate representation of the membrane for processes in which partitioning into the hydrocarbon phase is the main factor determining the energetics, and (iii) the dynamics of octane is orders of magnitude faster than that of phospholipids. Clearly, octane lacks a number of important features of real membranes, including (i) phospholipid headgroups and the associated charge distribution, (ii) the structured long lipid tails, and (iii) the non-uniform density and pressure profiles of real lipid bilayers. It would be of great interest to develop methods to incorporate these three features in simplified membrane models, both in mean field models and in our current model.

Analyses

All simulations and analyses were done with GROMACS programs. Secondary structure analyses use the definition of DSSP (Kabsch and Sander, 1983). Molecular graphics were made using Molscript (Kraulis, 1991). Hydrogen bonds were defined geometrically: the angle donor-hydrogen-acceptor has to be less than 60 degrees, the hydrogen-acceptor distance has to be less than 0.25 nm. Helix tilt angles were calculated as the angle between the normal on the octane or lipid layer and the line joining the centers of geometry of the first and last 7 Cα-carbons of a helix. Kink angles were calculated as the angle between the line joining the average Cα position of the first 4 N-terminal residues and the average Cα position of the last 3 residues before a pivot residue and the line joining the average coordinates of the 4 Cα atoms after the pivot and the average position of 3 Cα atoms at the N-terminus. As pivot residue we used Pro14, but the calculated kink angles are fairly insensitive to the choice of pivot, and Leu12 or Gly11 give very similar results. Root mean square deviations (RMSDs) were calculated for the backbone heavy atoms after fitting the Cα carbons to the initial model structure.

RESULTS

Alm at a POPC/water interface

In Fig. 3 the secondary structure of Alm at the water/lipid interface is given. It indicates a degree of variation between simulations that one might not expect given the small changes in simulation conditions. Alm-/POPC/0.66 is relatively stable and only shows fluctuations in the C-terminus, with reversible loss of helical structure in roughly the last 7 residues. Alm/POPC/0.66 rapidly loses its helical structure in the C-terminal two-thirds of the peptide, with mostly turn and, near the center of the peptide, coil formation. The N-terminal residues remain helical. The RMSD is more than 0.5 nm (graph not shown). In the Alm-/POPC simulation interesting fluctuations between turn, 3_{10} and α-helix occur, but overall the peptide loses all of its structure in 10 ns. Loss of secondary structure is reflected in the stepwise increase in the RMSD, through 0.2 nm, 0.3 nm, 0.4 nm to a maximum RMSD of 0.45 nm (graph not shown). In all three simulations, the changes in RMSD and secondary structure are concomitant with obvious changes in hydrogen bonding patterns, including loss of interhelical hydrogen bonds and an increase in water-protein hydrogen bonds. Lipid-protein hydrogen bonding occurs but is almost negligible compared to protein-protein and protein-solvent hydrogen bonds (details not shown).

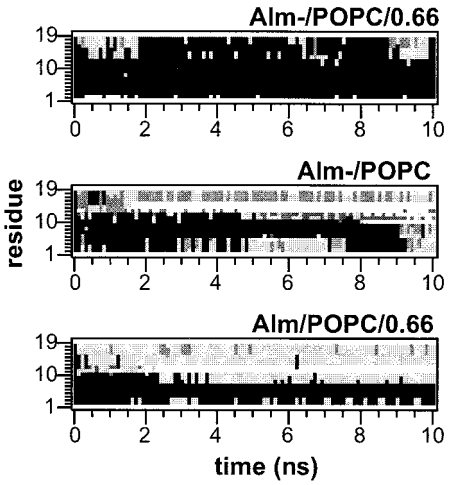

FIGURE 3 Secondary structure of alamethicin in the three simulations at the water/phospholipid interface. For the color legend, see Fig. 5. The *y*-axis runs from Aib1 to Gln19.

Over the course of 10 ns, the distance from the center of mass of the peptide to the center of mass of the lipid bilayer decreases about 0.1 to 0.2 nm for Alm-/POPC/0.66 and Alm-/POPC, about 0.4 nm for Alm/POPC/0.66, although in the latter the peptide unfolds nearly completely (graph not shown). The location in the bilayer can be seen in Fig. 4 (for Alm-/POPC). The peptide is distributed over ~1.5 nm, with the maximum density about 1 nm away from the maximum of the glycerol moiety distribution. Although there is significant overlap with the lipid distribution, the penetration into the lipid bilayer is shallow, and the depth of the peptide in the bilayer does not significantly change in 10 ns.

The apparent inconsistency of the results between the three simulations of Alm at a POPC/water interface may reflect the slow dynamics of the peptide in a phospholipid environment. In order to explore this aspect further, we have conducted a number of simulations at an octane/water interface, as the dynamics of this system is likely to be faster.

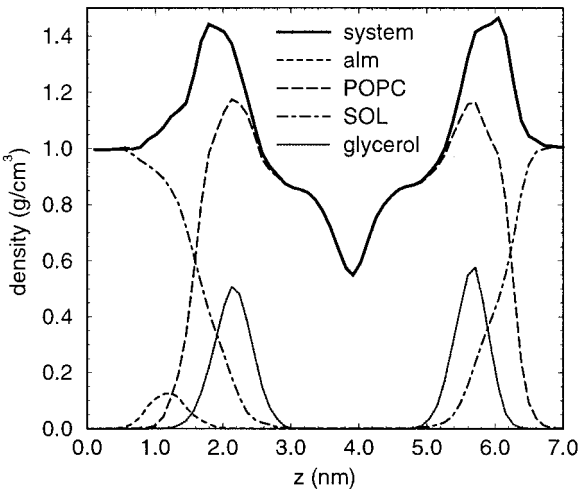

FIGURE 4 Density profile of the Alm-/POPC/0.66 simulation averaged over 10 ns, showing the distribution of the peptide, the lipid glycerol moiety, solvent, lipid, and of total system.

Octane/water simulations

Stability and secondary structure

Overall the helical secondary structure of alamethicin is preserved in all simulations with octane, and less stable in water (Fig. 5). However, there are some interesting details. In the surface bound Alm almost all of the fluctuations occur in the last C-terminal residues. On several occasions in the longer Alm simulations the peptide loses much of its structure for up to a nanosecond, only to refold back into a regular helix (e.g., Alm/0.1 at 41 ns). Such unfolding/refolding events almost always occur at the C-terminus and show as peaks in Fig. 6. The largest peak in Fig. 6, in Alm/0.1 at 93 ns, corresponds to the peptide temporarily breaking in the middle and collapsing onto itself, while maintaining a helical conformation at both termini. The inserted alamethicin helices show less fluctuation and a lower RMSD than the surface-bound alamethicin helices. Much of the time the RMSD with respect to the starting model is as low as 0.05 nm, although frequent and reversible excursions to considerably higher values occur. At the higher applied fields of 0.33 and 0.50 V/nm, the structure changes slightly, with some variation in the C-terminus.

In water, loss of helical structure occurs regularly near the middle of the peptide, where water molecules form hydrogen bonds with Aib10 and Gly11, disturbing the local structure. Similar behavior was found in simulations of Alm by Gibbs et al. (1997). In one of the three simulations of Alm in water the RMSD is 0.7 nm (Fig. 7), corresponding to an unfolded C-terminus. In the other two simulations in water, the middle of the peptide is disturbed. The RMSD after 2.5 ns is 0.4 nm, comparable to the RMSD for the poly-alanine helix in water after 2.5 ns. Thus, although Aib is helicogenic, its presence in the C-terminal half of the Alm molecule does not hold it in a rigidly α-helical conformation in water, but allows a local folded-unfolded equilibrium to occur. This is similar to the behavior of a polyalanine helix.

In water, the polyalanine termini show reversible loss of structure, and for a few hundred picoseconds a π-helix is formed locally. π-Helix formation has been implicated in helix unfolding and has been observed in other simulations (Korzhnev et al., 1999). In octane, the secondary structure of polyalanine remains almost completely α-helical, whether inserted or surface-bound (Fig. 5). The RMSD

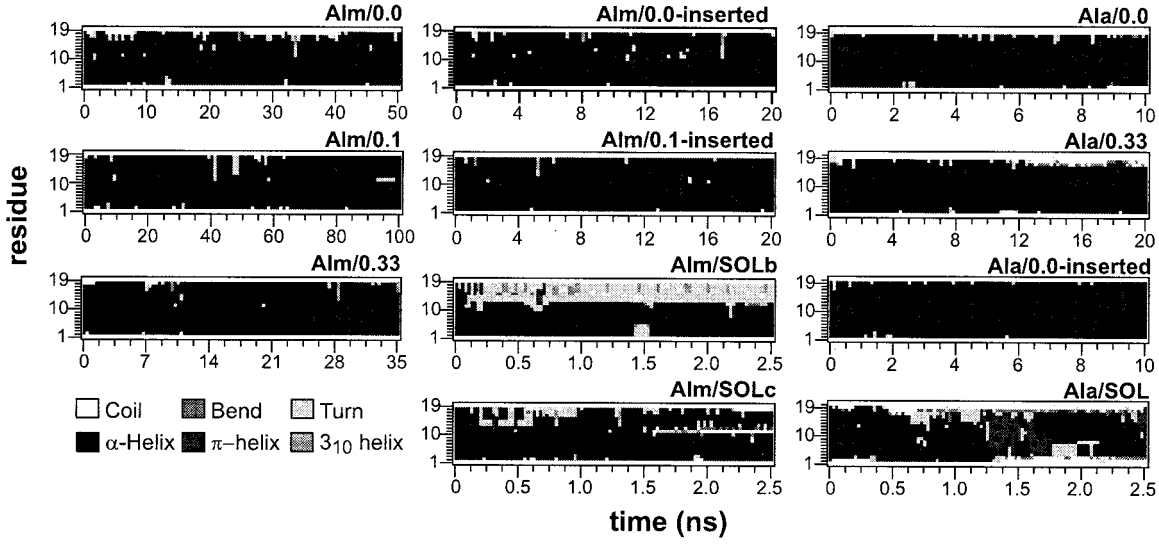

FIGURE 5 Secondary structure as function of time for a number of Alm and Ala simulations in water and octane. Note the different resolutions of the graphs, which have the same number of data points for simulations between 2.5 and 100 ns. π-helix only occurs in Ala/SOL and briefly in Alm/SOLb, 3_{10} helix only transiently in Alm/octane simulations. The *y*-axis in all graphs runs from Aib1 to Gln19.

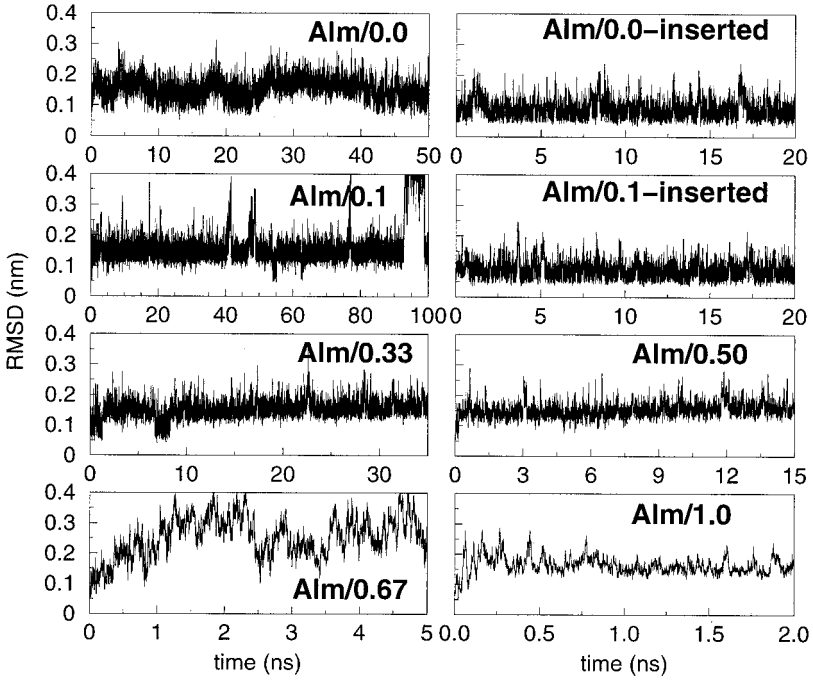

FIGURE 6 Root mean square deviations of the backbone, fitted on Cα-carbons, from the starting structure in a number of Alm/octane systems.

from the starting model shows relatively low values with reversible changes after excursions that can last several nanoseconds.

Orientation and mobility

To get an impression of the mobility of a peptide at the water/octane interface, in Fig. 8 the location of the center of mass of Alm over the 50 ns of the Alm/0.0 simulation is plotted. The peptide covers the entire plane of the interface, crossing the box several times, taking into account the periodic boundary conditions. The lateral diffusion coefficient, calculated from the mean square displacement of the center of mass of the peptide in the *x*,*y* plane over 10 ns, is $\sim 4 \times 10^{-10}\mathrm{m}^2\mathrm{s}^{-1}$. This may be compared with the experimentally measured diffusion coefficient of Alm in a lipid bilayer of $\sim 4 \times 10^{-11}\mathrm{m}^2\mathrm{s}^{-1}$, one order of magnitude smaller (Helluin et al., 1997). Note that the orientation of

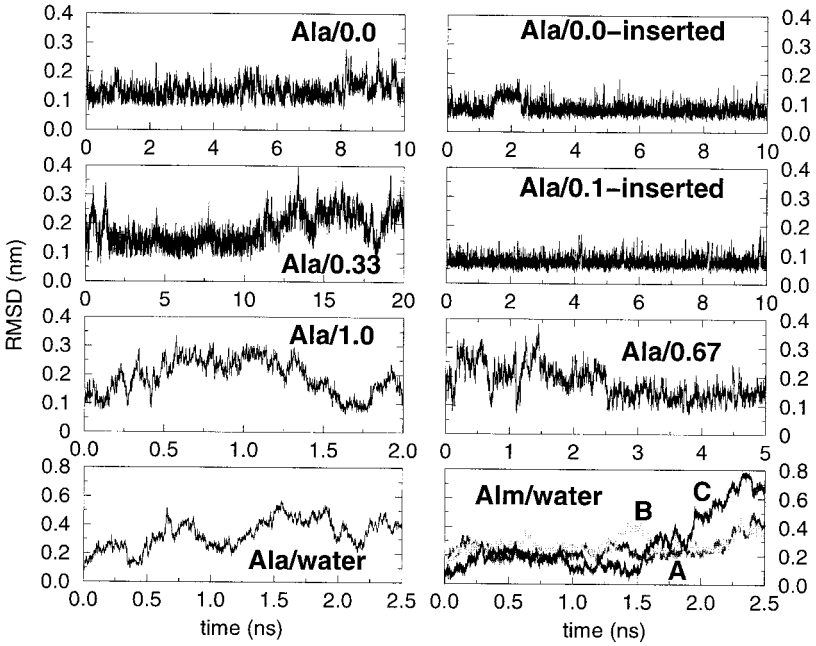

FIGURE 7 Root mean square deviations of the backbone, fitted on Cα-carbons, from the starting structure in poly-alanine and Alm/water systems.

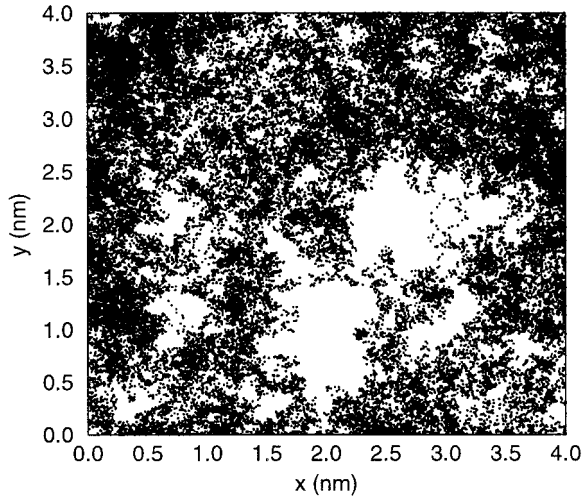

FIGURE 8 Diffusion of Alm/0.0 at the octane/water interfacial plane: the position of the center of mass of the peptide, represented by a black dot, during 50 ns.

Alm in this case is not known. The diffusion coefficient of Alm in the POPC simulations is too small to be calculated accurately from a 10-ns simulation, which is to be expected when considering the experimental value. For comparison, the lateral diffusion coefficient in the *x*,*y* plane of octane in the simulations is $\sim 3 \times 10^{-9} m^2 s^{-1}$.

In Fig. 9, the density profiles for the different components of inserted Alm peptide systems given for different field strengths. The peptide distribution is nearly independent of the external field, although there are some small differences between low and high fields. The peptide density is much higher at the C-terminus than at the N-terminus. This reflects the presence of the hydrophilic residues near the C-terminus that are anchored in the water phase, and the bulky Phl residue. A similar picture was found in simulations of an inserted alamethicin helix in POPC (Tieleman et al., 1999c). An additional factor is the mobility of the N-terminus in the octane slab, which undergoes significant motion as the helix changes tilt angle (see below), while the C-terminus is fixed by hydrogen bonding with water.

The width of the Alm helix distribution at the water/octane interface (Fig. 10) is the same as in Alm/POPC. The peptide partitions in the overlap region between solvent and hydrocarbon. If it is assumed that in a phospholipid bilayer this area is formed by the glycerol/carbonyl region, which seems a reasonable assumption, then the peptide binds in the same region as the amphipathic helix in the diffraction study of Hristova et al. (1999). Interestingly, the poly-alanine helix distribution almost completely overlaps with the Alm, taking into account its slightly lower mass and lack of long side groups. The external field has no discernible effect on the density profiles for the surface-bound peptides; the profiles for Ala/0.0 and Ala/0.33 overlap nearly perfectly (graph not shown).

In Fig. 10 *B*, details of the distribution of the different amino-acids are given in the inserted structure. The Phl residue has the broadest distribution, reflecting both its amphipathic nature with its hydrophilic end group and its aromatic side group and its location at the generally more flexible C-terminus. Most of the hydrophobic groups are facing the hydrocarbon exterior, with some necessary exceptions due to the low number of hydrophilic residues (e.g., Val15). Most of the hydrophilic residues and the exposed backbone carbonyls of residues Aib10 and Gly11 are facing the aqueous phase.

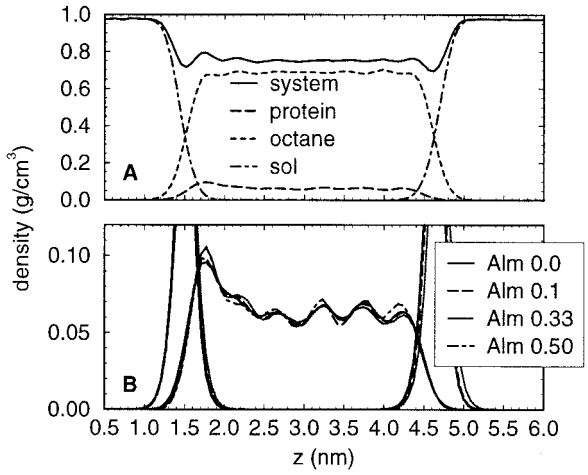

FIGURE 9 (*A*) Typical density profile for an inserted alamethicin: Alm/0.0-inserted. The C-terminus is located between 1.5–2 nm. (*B*) Distribution of alamethicin amino acids as function of the applied external field. The data are averaged over the entire simulation lengths for Alm/0.0/ins, Alm/0.1/ins, over 20–35 ns for Alm/0.33, and over 10–15 ns for Alm/0.50.

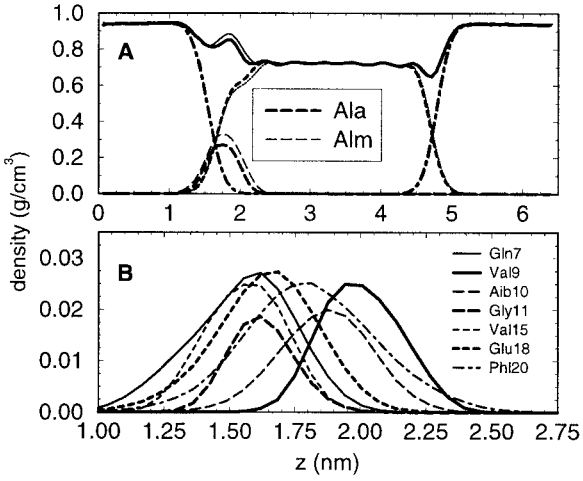

FIGURE 10 (*A*) Typical density profile for surface-bound peptide, Alm/0.0 and Ala/0.0. The curves nearly coincide, with the only noticeable difference the height of the peptide peak, due to the larger mass of Alm compared to Ala. (*B*) Detailed distribution of selected alamethicin amino acids.

Simulations of Alm inserted into the octane slab with 0.0, 0.1, 0.33, 0.50 V/nm, and higher applied fields allow a comparison of the distribution of tilt and kink angles as a function of the applied field. In Fig. 11 these distribution functions are shown. The tilt angle distribution becomes narrower and shifts toward 0 degrees (parallel to the *z*-axis) going from 0.0 to 0.50 V/nm. The difference between Alm/0.33 and Alm/0.50 is small. The maximum in the tilt angle distribution lies near 10 degrees, aligned with the external field. The distributions for Alm/0.0 and Alm/0.1 have broader maxima at a smaller angle. The tilt angle for poly-alanine at 0 V/nm is similar to the value for alamethicin. It is interesting to see that in one instance during the 20-ns simulation of the inserted Alm/0.0, the peptide actually changes tilt angle so much that it drags a number of water molecules into the octane phase. This is shown graphically in Fig. 12. At 12,600 ps, two water molecules are drawn into the octane phase by hydrogen bonding to the N-terminus. A few hundred picoseconds later, the exposed backbone around Aib10 and Gly11, as well as the side chain of Gln7, form hydrogen bonds with the *cis*-face water, while the N-terminus remains connected to the water at the other face. After 13,000 ps, the peptide returns to its orientation mostly perpendicular to the interfaces.

The kink angle calculated around Pro14 has a maximum at 30 degrees at all values of the applied electric field, although the distribution is slightly broader at 0.0 and 0.1 V/nm. In contrast to alamethicin, poly-alanine is hardly kinked, even at no external field. Higher external fields only stabilize the helix more in a straight conformation.

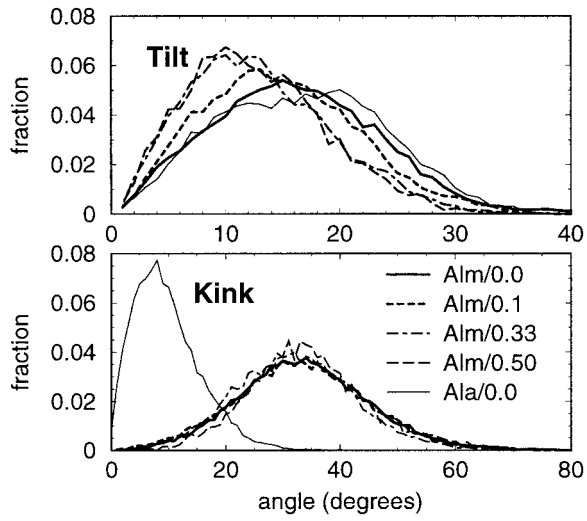

FIGURE 11 Distribution of tilt (*top*) and kink angles (*bottom*) for Alm/0.0-inserted, Alm/0.1-inserted, the 20–35 ns part of the trajectory of Alm/0.33, the 10–15 ns part of Alm/0.50, and the Ala/0.0-inserted simulations. A tilt angle of 0 degrees corresponds to perfect alignment of the helical axis with the z-axis.

Helix dipole moments

The Alm and Ala helices have no charged residues, but the total dipole moment of a helix is quite large (Hol, 1985). The total helical dipole moment is expected to depend on the external field, because the external field, because the external field will stabilize structures with a high dipole moment aligned with the external field. Indeed, for the inserted Alm peptides, the average total dipole moments are 59.8 ± 3 D for 0 V/nm, 60.4 ± 3 D for 0.1 V/nm, 61.4 ± 3 D for 0.33 V/nm, 62.3 ± 4 D for 0.50 V/nm, 54.4 ± 4 D for 0.67 V/nm, and 65.8 ± 3 D for 1.0 V/nm. These values can be compared with a value of 55.3 D for the initial model. The average dipole moment for surface-bound Alm without external field is 59.3 ± 4 D. We calculated 68.5 D, 66.1 D, and 65.1 D for the three monomers in the crystal structure of Fox and Richard (1982). In all cases the partial charges from the GROMOS96 force field were used. For the crystal structures, hydrogen positions were generated based on ideal geometries, without energy minimization. Clearly, the total dipole moment increases with applied field, ignoring the outlier at 0.67 V/nm. One would expect a saturation effect of the total dipole moment as function of the external field, but this is not observed. The change in conformation of the peptide is quite subtle and includes both changes in the overall kink angle and small local adjustments.

Insertion into the octane phase

In the Alm/0.0 and Alm/0.1 simulations, Alm does not insert spontaneously in the octane phase in 50 ns and 100 ns, respectively. Furthermore, inserted structures simulated for 20 and 10 ns at 0 and 0.1 V/nm, respectively, showed no tendency to change orientation from transmembrane to surface-bound. At higher field strengths, Alm does insert into the octane phase. In Alm/0.33, the insertion process takes about 2 ns, occurring between ~16 and 18 ns into the simulation. At 0.50 V/nm, the insertion process takes place between 7.5 and 8.5 ns. At 0.67 V/nm, insertion occurs between 500 and 800 ps. At 1.0 V/nm, insertion occurs nearly immediately, between 0 and 500 ps. Finally, at 2.0 V/nm, insertion occurs between 0 and 200 ps.

Polyalanine only inserted in the Ala/1.0 simulation, from about 500 to 600 ps into the simulation. No insertion occurs at 0.33 V/nm during 20 ns of simulation or at 0.67 V/nm in 5 ns of simulation. It is also possible at −1.0 V/nm or more to insert Alm with its C-terminus. However, this entails severely disrupting the octane slab, and a large number of water molecules is dragged into the hydrophobic phase.

The insertion process can be monitored visually (Fig. 13) through a number of critical hydrogen bonds (Fig. 14 and Table 2), and through the total dipole moment as well as μ_z, the *z* component of the total dipole moment of the Alm molecule.

In Fig. 13 snapshots of the insertion process of Alm/0.33 are given at 250-ps intervals, starting at 15,125 ps. In the

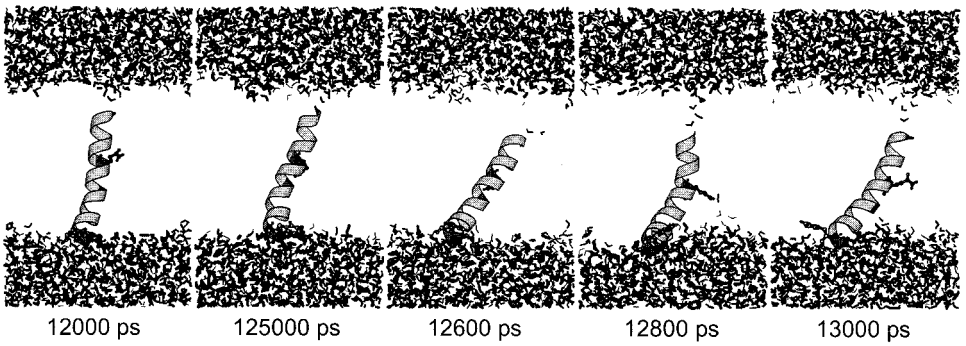

FIGURE 12 Snapshots covering 1 ns of Alm/0.0-inserted.

first three snapshots, the peptide assumes various orientations at the octane/water interface. In the fourth snapshot the N-terminus of the peptide is somewhat inserted into the octane, but the Gln7 side group is still hydrogen-bonded to the water phase. This conformation alternates a few times with a more parallel surface-bound orientation, but the N-terminal insertion becomes more pronounced at 16,125 and 16,375 ps. Somewhere between 16,375 and 16,450 ps, the hydrogen bonds between water and the Gln7 side chain break, and the peptide continues to insert more deeply. The loss of hydrogen bonding between water and Gln7 is clearly visible in Fig. 14 at ~1000 ps in the graph, corresponding to 16,500 ps for Alm/0.33 and 8000 ps for Alm/0.50. It also corresponds to the plateau region in Fig. 15 for μ_z, the peptide dipole moment along the normal to the octane/water interface. As the insertion process continues, the next critical interactions determining the process are hydrogen bonding interactions between water and the Aib10 and Gly11 backbones. In Fig. 14 it is clear that both these residues are going to lose one hydrogen bond by going from a surface-bound to inserted orientation of the peptide. In the snapshots this is translated to a structure in which the C-terminal half of the peptide attempts to remain near the water/octane interface. Water molecules occasionally penetrate slightly into the octane phase, and the hydrogens are broken and reformed. But in the end, at 17,125 ps and onward, the hydrogen bonds between Aib10 and Gly11 are lost, and the peptide inserts completely. The total dipole moment and its *z* component become nearly identical (Fig. 15). Interestingly, the helix kink angles fluctuate during the insertion in Alm/0.33 and Alm/0.50, but not significantly more or less than during the rest of the simulation, and no significant change is observed. A less noisy view of the change in kink angle can also be inferred from the total dipole moment. However, the fluctuations in the total dipole moment during the insertion process are difficult to distinguish from fluctuations during parts of the trajectory where the peptide is surface bound or inserted. There is no evidence for an increase in kink angle during the insertion process. Finally, the last five snapshots give an impression of the different conformations and orientations in the octane slab that the peptide assumes during 1.5 ns (see also below).

Internal hydrogen bonding

Although alamethicin is a relatively simple molecule, the presence of Aib residues and the proline at position 14 cause significant deviations from an ideal α-helical structure (Sansom, 1991; Gibbs et al., 1997). In Table 2, a summary of hydrogen bonding for a number of residues is given for Alm/0.33 and Alm/0.50 during the 3 ns of the insertion process (15,500–18,500 ps for Alm/0.33, 7000–10,000 ps for Alm/0.50). The hydrogen bonding patterns are remarkably similar, reinforcing the picture drawn from Figs. 14 and 15 that the insertion processes for Alm/0.33 and Alm/0.50 are very similar, although the latter is faster. The table shows the incomplete hydrogen bonding for the Aib10 and Gly11 carbonyl oxygen, both due to the presence of Pro14. This is a general feature and similar proportions are found in all simulations of inserted Alm. A significant fraction of *i*, *i* + 3 backbone hydrogen bonding occurs in all residues shown, between 2% and 25% of the time.

DISCUSSION

Peptide stability

The simulations of Alm on a phospholipid bilayer show that Alm has a fluctuating secondary structure in the water/outer headgroup region of the bilayer. The phospholipid simulations clearly show the much longer time scales of peptide motion, and the need for the development of more advanced methods to study the interactions between surface-bound peptides and phospholipids. However, on a water/octane interface, mimicking the water-headgroup-carbonyl/hydrocarbon interface in the lipid bilayer, Alm is very stable as a helix.

Ladokhin and White (1999) measured the free energy contribution of the formation of helical secondary structure for mellitin and found a value of 1.7 kJ mol^{-1} per residue. Wieprecht et al. (1999), using magainin and magainin-derivatives with D-amino acids, determined a smaller value of about 0.8 kJ mol^{-1} per residue. This favorable free energy arises almost entirely from hydrogen bonding interactions of the backbone carbonyl and amide groups. For a 20-residue peptide like alamethicin, this would amount to a

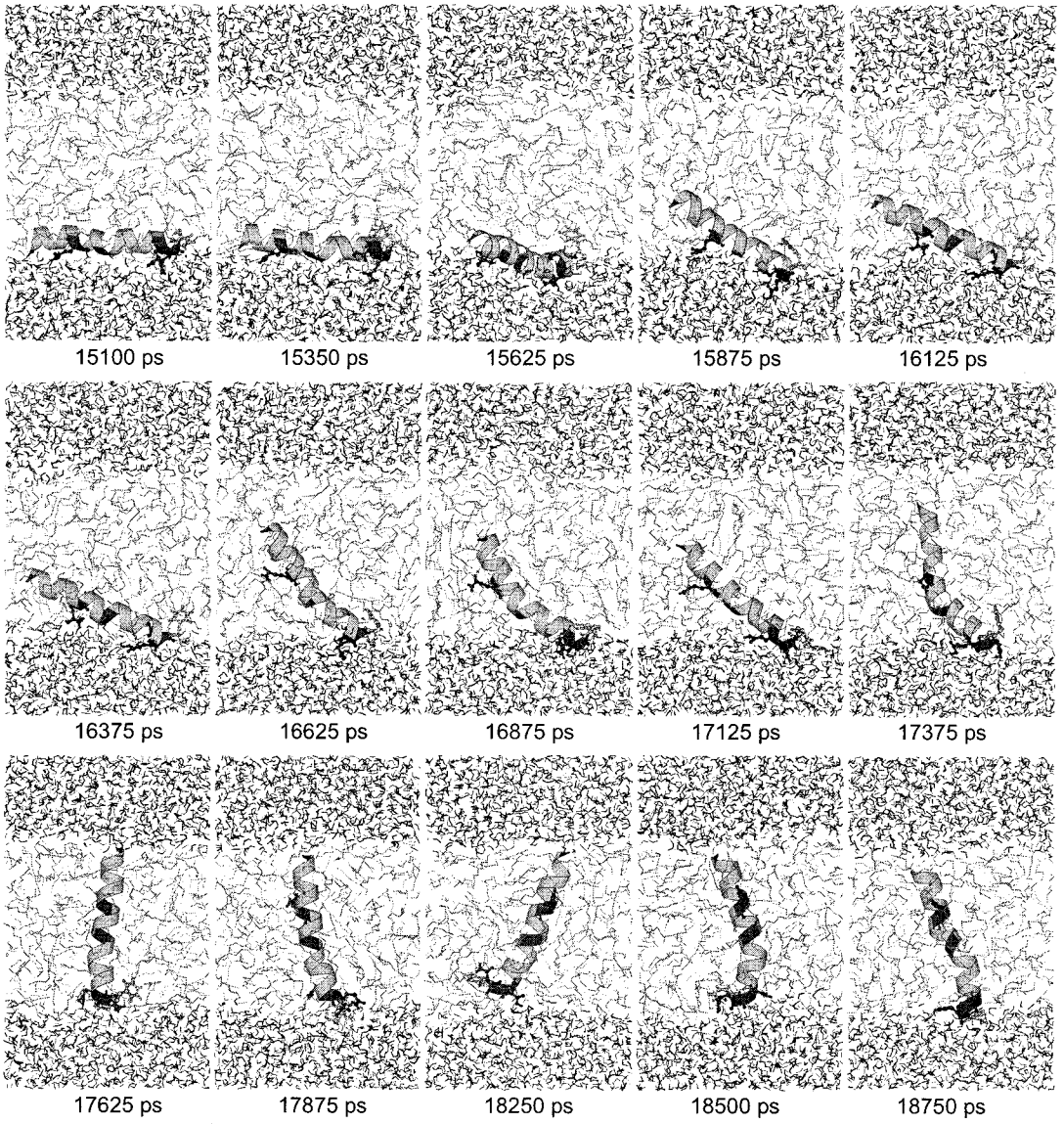

FIGURE 13 Snapshots during the insertion process of Alm/0.33. Gln7, Gln18, Glu19, and Phl20 are drawn as ball-and-stick. Gly11 and the N-terminus are dark grey.

substantial energy of about 34 kJ mol^{-1}, or 14 *kT*. With the values from Wieprecht et al., the free energy difference would still be 7 *kT*. In this light the stable secondary structure and low RMSD values for both Alm and Ala bound to and inserted in octane are logical. However, it is also clear that thermal fluctuations are sufficient for large but transient disturbances in the structure of the peptides. Such disturbances in Alm are almost always C-terminal, and can involve reversible loss of secondary structure of the C-terminal half of the peptide. Inserted into the octane slab, there is some fluctuation near the C-terminal residues. Most structural studies on Alm have suggested that the N-terminus is more stable than the C-terminus, which from EPR spectroscopy seems to be located in the lipid headgroup region (Barranger-Mathys and Cafiso, 1996; Franklin et al., 1994), whereas the N-terminus is within the hydrophobic membrane interior. This is consistent with the results from our simplified membrane.

Orientation and insertion

Alm rapidly binds at the water/octane interface. Interestingly, the poly-alanine helix binds at exactly the same depth as Alm at the octane/water interface. If Alm would be positioned deeper inside the phospholipid bilayer, near the carbonyl groups, it seems likely that it will be stabilized in a similar fashion as in octane/water. Although there is no

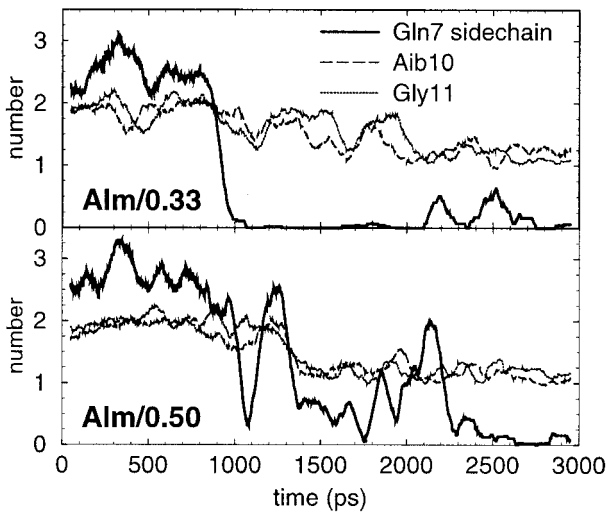

FIGURE 14 Critical hydrogen bonding between residues and the rest of the system during the insertion process for Alm/0.33 (*top*) and Alm/0.50 (*bottom*): Gln7 (side chain only), Aib10, and Gly11. $t = 0$ in the graphs corresponds to 15,500 ps for Alm/0.33, to 7000 ps for Alm/0.50. Data are running averages over 100 ps.

TABLE 2 Overview of the different hydrogen bonds occurring between protein atoms during 3 ns, including the insertion process for Alm/0.33 and Alm/0.50

			Alm/0.50	Alm/0.33
		Gln7		
Gln7-N	Gln7-H	Aib3-O	2815	2784
Gln7-N	Gln7-H	Ala4-O	172	201
Gln7-NE2	Gln7-HE21	Aib3-O	230	176
Gln7-NE2	Gln7-HE21	Ala4-N	4	5
Gln7-NE2	Gln7-HE21	Ala4-O	7	3
Aib10-N	Aib10-H	Gln7-O	49	63
Gly11-N	Gly11-H	Gln7-O	2547	2606
		Gln7 internal		
Gln7-NE2	Gln7-HE21	Gln7-O	395	162
Gln7-N	Gln7-H	Gln7-OE1	0	1
Gln7-N	Gln7-H	Gln7-NE2	0	1
		Aib10		
Aib10-N	Aib10-H	Ala6-O	2850	2868
Aib10-N	Aib10-H	Gln7-O	49	63
Aib13-N	Aib13-H	Aib10-O	352	328
		Gly11		
Gly11-N	Gly11-H	Gln7-O	2547	2606
Gly11-N	Gly11-H	Aib8-O	774	638
Gly11-N	Gly11-H	Val9-O	10	11
Val15-N	Val15-H	Gly11-O	759	668
Aib16-N	Aib16-H	Gly11-O	29	0
		Leu12		
Leu12-N	Leu12-H	Aib8-O	2747	2750
Leu12-N	Leu12-H	Val9-O	410	469
Val15-N	Val15-H	Leu12-O	244	280
Aib16-N	Aib16-H	Leu12-O	2800	2787
Aib17-N	Aib17-H	Leu12-O	43	0
		Pro14		
Aib17-N	Aib17-H	Pro14-O	160	159
Glu18-N	Glu18-H	Pro14-O	2618	2713
Glu18-OE2	Glu18-HE2	Pro14-O	95	0

Note that hydrogen bonds are listed per residue, so that there is some redundancy in the table. The numbers after each hydrogen bond are the number of time frames (3000 total, 1/ps) in which the hydrogen bond exists in Alm/0.50 and Alm/0.33.

experimental structural evidence for the depth of binding of surface-bound Alm to lipids, Hristova et al. have determined the location of membrane binding peptides in dioleoyl-phosphatidylcholine (DOPC) bilayers using an X-ray diffraction method (White and Wimley, 1998; Hristova et al., 1999). They found that their model amphipathic helix could be fit to a density distribution with the maximum coinciding with the maximum of the glycerol moiety density in the lipid bilayer. Although this location might differ among different helices, it is also roughly the location predicted by simulations of part of dermaseptin S3 and an antimicrobial model peptide MB21 (Tieleman, D. P., unpublished), as well as Alm and Ala in this study. These results suggest that octane can be useful to predict the orientation of membrane binding peptides, which is of general use in studying membrane-bound peptides. However, it should be kept in mind that the distributions of functional groups in phospholipid bilayers are much wider than in alkane/water interfaces.

It is still an unresolved issue whether Alm is surface-bound or inserted without the presence of a membrane potential. According to CD and Raman spectroscopy, Alm is inserted under most conditions, but at low temperature or hydration it is surface-bound (Vogel, 1987). Huang et al. showed using X-ray diffraction that Alm is surface-bound in diphytanoylphosphatidylcholine at low concentrations (Huang and Wu, 1991; Wu et al., 1995) but inserts at higher concentration (ratio of more than 1/40 peptide/lipids) and forms pores. Using the same X-ray diffraction method, it was shown that the critical concentration where the shift between inserted and surface-bound occurs can be modulated by the presence of lipids that induce curvature stress (Heller et al., 1997). Solid state NMR at high peptide concentration showed that Alm inserts and is α-helical at the N-terminus when inserted (North et al., 1995), in agreement with electron paramagnetic resonance spectroscopy data that suggested that Alm may not completely span the bilayer but is mostly inserted (Barranger-Mathys and Cafiso, 1996). At a peptide concentration of 0.25–0.50 mole percent, alamethicin was found to be predominantly transmembrane in POPC at 95% relative humidity by solid state NMR (B. Bechinger, Max Planck Institute for Biochemistry, personal communication). Older data has been reviewed by Woolley and Wallace and, although conflicting data exist, seem to point to a significantly inserted fraction of

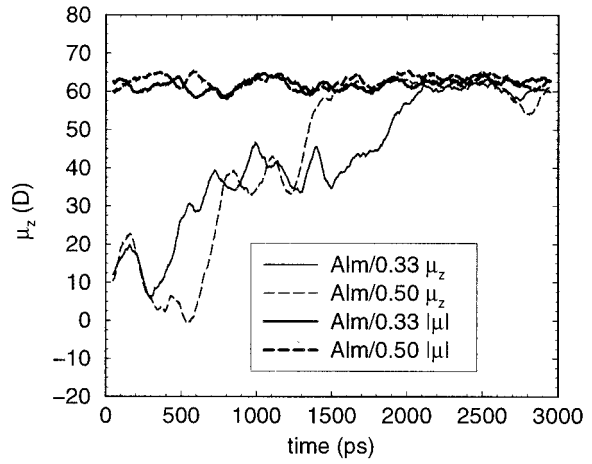

FIGURE 15 Change in the total dipole moment of the Alm peptide and its *z* component during the insertion Alm/0.33 and Alm/0.50, taken as 100-ps running averages. $t = 0$ in the graph corresponds to 15,500 ps for Alm/0.33, to 7000 ps for Alm/0.50. Data are running averages over 100 ps.

Alm (Woolley and Wallace, 1992). Finally, amide-resolved hydrogen-exchange measurements of Alm in the presence of DOPC vesicle confirmed that the peptide is mostly helical along the entire sequence but were unable to distinguish between a surface-bound and an inserted orientation (Dempsey and Handcock, 1996).

Recent continuum solvent calculations (Kessel et al., 2000) showed that for a 3.0 nm wide low dielectric slab, the inserted conformation was more favorable than surface-bound by 2.5 to 4.5 kJ/mol. If the slab was allowed to deform locally, the difference increased to 6 to 8.5 kJ/mol. At a larger hydrophobic thickness, surface-bound became more favorable; at a smaller thickness, the inserted orientation. Both surface-bound and inserted orientations are much more favorable than solvation in water. These free energy differences suggest that there will be a small but possibly measurable fraction of Alm surface-bound, with the majority being inserted.

The same calculations also show that there is a barrier for insertion of the crystal conformations (Fox and Richards, 1982) along the bilayer normal of about 40 kJ/mol for N-terminal insertion of the Alm crystal structures, about 80 kJ/mol for C-terminal insertion (Kessel et al., 2000), and much larger barriers for the NMR structures with their incomplete helical hydrogen bonding (Franklin et al., 1994). This illustrates the importance of the graphical view of the insertion process presented in this study, emphasizing the structural changes that occur during insertion. It seems likely that the actual barriers for insertion are significantly smaller when taking the dynamic structure of Alm into account, that on a nanosecond time scale allows partially unfolding and refolding. Taking these theoretical and experimental results into account, it is not surprising that Alm is stable as a helix at no or low applied field, whether the peptide is surface-bound or inserted.

We are able to identify the dehydration of the Gln7 side chain as one major factor and the dehydration of the Aib10 and Gly11 backbone carbonyls as a second major factor resisting insertion. Both the inserted and surface-bound orientations are highly stabilized compared to Alm in aqueous solution. In order to calculate the relative free energy difference from the current simulations, we would need either a complicated free energy calculation or many transitions between inserted and surface-bound states in a single simulation. Many transitions would also be required for kinetic analyses to estimate the barrier height. Therefore, we cannot determine from these simulations what the most favored orientation is.

However, the added field in the simulations gives some indication about the relative energies involved. The energy U_e of a dipole μ in a field E is $U_e = -\mu \cdot E$. With $\mu \sim 50$ D and $E_z = 0.1$ V/nm, $U_e = -10$ kJ/mol. This extra term makes the inserted orientation more favorable by an additional 10 kJ/mol. At fields of 0.33 V/nm and higher, Alm inserts faster with higher field. At a field of −1.0 V/nm and higher, C-terminal insertion occurs too (although it might occur at lower fields, given enough time), but this involves an extra energy of 100 kJ/mol, enough to severely distort the octane slab. In addition, at a field of more than 1 V/nm, the octane slab becomes unstable, with increased water permeation. This may have interesting implications with respect to electroporation. A field of 0.33 V/nm across an octane slab of 3 nm, plus a much smaller field across an additional 3 nm of solvent, corresponds to a potential difference of roughly 1 V across the membrane. This is much larger than the 100–250 mV typical under physiological conditions and experiments but, given the very large fields and potential fluctuations at the atomic scale, not too dramatic. The emphasis in the analyses in this paper is on calculations at 0, 0.1 and 0.33 V/nm.

Alamethicin has three distinguishing features compared to a regular poly-alanine helix. *i*) Around the Aib-Gly-X-X-Pro sequence, α-helical hydrogen bonding is, by necessity, distorted. The carbonyl group of Aib10 cannot form a hydrogen bond with Pro14, and the carbonyl group of Gly11 is exposed. *ii*) The side group of Gln7 cannot form hydrogen bonds when Alm is inserted in the hydrocarbon phase. *iii*) The Glu18-Gln19-Phl20 at the C-terminus is likely to form a disturbed secondary structure, with all three residues predominantly in the aqueous phase, but the phenyl group of Phl in the octane phase. Alamethicin also has a more kinked structure than poly-alanine. Although during insertion no significant changes in kink angle are observed, the normal range of kink angles induced by the Alm sequence (over 90% between 5 and 40 degrees for Alm/0.0) does support the insertion in two steps observed in the simulations. The total dipole moment and helical secondary structure are preserved during the insertion processes. Interestingly, the presence of Pro14, although partially responsible for inducing the bend structure, also causes the 'unfavorable for insertion' exposed backbone atoms at Aib10 and Gly11.

Voltage-activated channels?

For over 20 years, different models have been made of how Alm forms voltage-activated channels. Although the current simulations do not describe channel formation, it is useful to compare the results with some of the proposed models (Woolley and Wallace, 1992; Sansom, 1991; Barranger-Mathys and Cafiso, 1996). It should be kept in mind that the experimental data were collected over a wide range of peptide concentrations, lipid types, salt concentrations, and other experimental conditions. There is some evidence that the mechanism of channel formation might not be exactly the same under different conditions.

Models that rely on major conformational changes induced by the electrostatic field are not well supported by the simulations, in all of which Alm is mostly α-helical throughout, in agreement with several experimental results. High resolution NMR of Alm in micelles (Franklin et al., 1994) and amide hydrogen-deuterium exchange measurements (Dempsey and Handcock, 1996) support a full helical structure in lipid environments. Partially inserted or unfolded monomers occur only rarely and transiently in the simulation. The distribution of kink and tilt angles depends on the external field (Fig. 11), but this effect is not very strong. A mechanism in which Alm is inserted but inserts further, under the influence of a potential difference, to form the active state has been suggested (Barranger-Mathys and Cafiso, 1996). The simulations do show some change in depth as a function of the field, as well as a change in kink and tilt angles. In particular, the tilt angle distribution at zero applied field is wider, and, in one event during the simulation, an inserted peptide came sufficiently close to the water/octane interface to form hydrogen bonds between its backbone and Gln7 side chain and water on the *cis* side. If the free energy change associated with the aggregation of already inserted helices is small, it is possible that such fairly subtle changes are required for aggregation to occur.

Flipflop models in which some alamethicin helices within an aggregate are oriented anti-parallel but switch to a parallel orientation seem unlikely in light of experimental evidence with covalently linked alamethicins (Woolley et al., 1997). In addition, a major reason for such models was the assumption that anti-parallel helices are much more favorable electrostatically than parallel helices. More recent calculations have shown that if the helices are solvated at their termini, this effect is actually small (Ben-Tal and Honig, 1996), and packing interactions dominate (Zhou et al., 2000; Choma et al., 2000).

Voltage-dependent insertion of peptides due to the interaction between the helical dipole and the transmembrane potential is an attractive idea. However, it appears that in many circumstances a significant fraction of Alm already is inserted in the bilayer without the application of an external field. It is still possible that at the very low concentrations used in electrophysiological measurements, a transmembrane voltage shifts the equilibrium between inserted and surface-associated helices towards inserted helices, in order to reach a critical concentration for channel formation.

Pre-aggregation of alamethicin on the surface of a bilayer and subsequent insertion as an aggregate or a complete pore has also been suggested as mechanism. Our current simulations do not address this mechanism, but there is indirect experimental data that is consistent with such a model (Woolley and Wallace, 1992).

A final class of models suggests that alamethicin aggregates in a voltage-dependent manner to form channels. If the energetic balance between monomers and aggregates is subtle, relatively minor conformational changes that change packing conditions might favor aggregation and channel formation. If this is the case, then effects that cannot be inferred with confidence from a single Alm molecule must play an important role. Interestingly, judging from EPR (Barranger-Mathys and Cafiso, 1996) and the current simulations, Alm can be considered solvated at the C-terminus, but much less so at the N-terminus. This makes Alm an intermediate case in the analyses of Ben-Tal and Honig (1996): with both termini solvated by water, the repulsive electrostatic interactions between two parallel transmembrane helices are small, but with both termini in the low dielectric bilayer interior, the repulsive interactions are very strong. In the case of alamethicin, the C-terminus seems well-solvated, whereas the N-terminus is much less solvated. A relatively small change in the depth of insertion, perhaps as suggested by the snapshots in Fig. 12, could make a significant difference in pore formation. This would also be in the spirit of the model proposed by Barranger-Mathys and Cafiso (1996). Based on the currently available experimental and theoretical evidence, voltage-dependent aggregation seems a serious candidate mechanism.

The simulations we present here are not sufficient to build a reliable model of channel formation. However, our results do allow a meaningful comparison of different models for channel formation and suggest that a subtle mechanism of channel formation merits further investigation. Although it is possible and interesting to study models of Alm bundles, such molecular models yield little useful information on the process of aggregation and channel formation (Tieleman et al., 1999a; Sansom et al., 1999). It will be an interesting challenge to apply both experiments and theory to study of the aggregation and channel formation process in more detail.

CONCLUSIONS AND OUTLOOK

We have described the structure and dynamics of Alm at the water/phospholipid and water/octane interfaces. The peptide does not move enough to find the most favorable position in 10 ns in the water/phospholipid interface and is not very stable 1 nm away from the maximum glycerol moiety density, delimiting the hydrophobic core of the membrane. However, the simulations in octane show a rich behavior of both alamethicin and poly-alanine at the water/octane interface and inserted into the octane phase. Indeed,

in spite of the large barrier to insertion, we observe the insertion of Alm at a field of 0.33 V/nm into the octane phase, allowing a first glance in atomic detail at such a process. The similarity between the insertion process at 0.33 V/nm and 0.50 V/nm leads us to believe the process will be very similar, although slower, at 0 or 0.1 V/nm.

It is exciting to follow the trajectory of alamethicin as it inserts into the hydrocarbon phase in atomic detail. The molecular motions in phospholipid are much slower, and it will be a while before a similar simulation of Alm with a phospholipid bilayer will show insertion, even at elevated fields. However, the simulations in octane give consistent and converged results. The molecular motions are rapid enough to hold promise as a means of studying aggregation of peptides at a simplified water/membrane interface, which we believe will be essential to understand the voltage-dependent channel formation of alamethicin. It will be of great interest to study other peptides, to combine the explicit simulations with continuum solvent calculations and detailed experimental thermodynamic measurements for model peptides (White and Wimley, 1999). The recent diffraction results of White and coworkers (Hristova et al., 1999) provide a benchmark system for computational procedures aimed at determining the preferred location of a peptide at a water/lipid interface. Many challenging opportunities for systematic studies of phospholipid bilayer-peptide interactions await. Establishing a methodology for studying voltage-dependent conformational changes will be of immense value for the near future, to study voltage activation of more complex channels such as the voltage-gated potassium channels (Sansom, 2000) after their structures become available.

D.P.T. thanks EMBO for a long term fellowship. Work in M.S.P.S.' group is supported by the Wellcome Trust.

REFERENCES

Arkin, I. T., P. D. Adams, C. F. C. Ludlam, S. Aimoto, K. J. Rothschild, A. T. Brunger, D. M. Engelman, and S. O. Smith. 1995. Structural model of the phospholambam ion channel in membranes. *Protein Eng.* 8:44.

Bachar, M., and O. M. Becker. 2000. Protein induced membrane disorder: a molecular dynamics study of melittin in a dipalmitoylphosphatidylcholine bilayer. *Biophys. J.* 78:1359–1375.

Barranger-Mathys, M., and D. S. Cafiso. 1996. Membrane-structure of voltage-gated channel forming peptides by site-directed spin-labeling. *Biochemistry.* 35:498–555.

Bechinger, B. 1996. Towards membrane protein design: pH-sensitive topology of histidine-containing polypeptides. *J. Mol. Biol.* 263:768–775.

Bechinger, B. 1999. The structure, dynamics and orientation of antimicrobial peptides in membranes by multidimensional solid-state NMR spectroscopy. *Biochim. Biophys. Acta.* 1462:157–183.

Ben-Shaul, A., N. Ben-Tal, and B. Honig. 1996. Statistical thermodynamic analysis of peptide and protein insertion into lipid membranes. *Biophys. J.* 71:130–137.

Ben-Tal, N., A. Ben-Shaul, A. Nicholls, and B. Honig. 1996. Free-energy determinants of alpha-helix insertion into lipid bilayers. *Biophys. J.* 70:1803–1812.

Ben-Tal, N., and B. Honig. 1996. Helix-helix interactions in lipid bilayers. *Biophys. J.* 71:3046–3050.

Berendsen, H. J. C., J. P. M. Postma, W. F. Gunsteren, and J. Hermans. 1981. Interaction models for water in relation to protein hydration. *In* Intermolecular Forces, B. Pullman, editor. Reidel, Dordrecht, The Netherlands. 331–342.

Berendsen, H. J. C., J. P. M. Postma, W. F. van Gunsteren, A. DiNola, and J. R. Haak. 1984. Molecular dynamics with coupling to an external bath. *J. Chem. Phys.* 81:3684–3689.

Berendsen, H. J. C., D. van der Spoel, and R. van Drunen. 1995. GROMACS: A message-passing parallel molecular dynamics implementation. *Comp. Phys. Comm.* 91:43–56.

Berger, O., O. Edholm, and F. Jähnig. 1997. Molecular dynamics simulations of a fluid bilayer of dipalmitoylphosphatidylcholine at full hydration, constant pressure, and constant temperature. *Biophys. J.* 72:2002–2013.

Bernèche, S., M. Nina, and B. Roux. 1998. Molecular dynamics simulations of melittin in a dimyristoylphosphatidylcholine bilayer membrane. *Biophys. J.* 75:1603–1618.

Biggin, P. C., J. Breed, H. S. Son, and M. S. P. Sansom. 1997. Simulation studies of alamethicin-bilayer interactions. *Biophys. J.* 72:627–636.

Cafiso, D. S. 1994. Alamethicin: a peptide model for voltage gating and protein membrane interactions. *Ann. Rev. Biophys. Biomol. Struct.* 23: 141–165.

Chang, G., R. H. Spencer, A. T. Lee, M. T. Barclay, and D. C. Rees. 1998. Structure of the MscL homolog from *mycobacterium tuberculosis*: A gated mechanosensitive ion channel. *Science.* 282:2220–2226.

Chipot, C., B. Maigret, and A. Pohorille. 1999. Early events in the folding of an amphipathic peptide: a multinanosecond molecular dynamics study. *Proteins Struct. Funct. Gen.* 36:383–399.

Chipot, C., and A. Pohorille. 1998. Folding and translocation of the undecamer of poly-L-leucine across the water-hexane interface, a multinanosecond molecular dynamics study. *J. Am. Chem. Soc.* 120: 11912–11924.

Choma, C., H. Gratkowski, J. D. Lear, and W. F. DeGrado. 2000. Asparagine-mediated self-association of a model transmembrane helix. *Nat. Struct. Biol.* 7:161–166.

Daura, X., K. Gademann, B. Jaun, D. Seebach, W. van Gunsteren, and A. Mark. 1999. Peptide folding: when simulation meets experiment. *Angew. Chem. Int. Edit.* 38:236–240.

Daura, X., B. Jaun, D. Seeback, W. F. van Gunsteren, and A. E. Mark. 1998. Reversible peptide folding in solution by molecular dynamics simulations. *J. Mol. Biol.* 280:925–932.

Dempsey, C. E., and L. J. Handcock. 1996. Hydrogen-bond stabilities in membrane-reconstituted alamethicin from amide-resolved hydrogen-exchange measurements. *Biophys. J.* 70:1777–1788.

Duan, Y., and P. Kollman. 1998. Pathways to a protein folding intermediate observed in a 1-microsecond simulation in aqueous solution. *Science.* 282:740–744.

Epand, R. M., and H. J. Vogel. 1999. Diversity of antimicrobial peptides and their mechanisms of action. *Biochim. Biophys. Acta.* 1462:11–28.

Esposito, G., J. A. Carver, J. Boyd, and I. D. Campbell. 1987. High resolution ^{1}H NMR study of the solution structure of alamethicin. *Biochemistry.* 26:1043–1050.

Feenstra, K. A., B. Hess, and H. J. C. Berendsen. 1999. Improving efficiency of large time-scale molecular dynamics simulations of hydrogen-rich systems. *J. Comp. Chem.* 20:786–798.

Fox, R. O., and F. Richards. 1982. A voltage-gated ion channel model inferred from the crystal structure of alamethicin at 1.5-Å resolution. *Nature.* 300:325–330.

Franklin, J. C., J. F. Ellena, S. Jayasinghe, L. P. Kelsh, and D. S. Cafiso. 1994. Structure of micelle-associated alamethicin from ^{1}H NMR. Evidence for conformational heterogeneity in a voltage-gated peptide. *Biochemistry.* 33:4036–4045.

Gibbs, N., R. B. Sessions, P. B. Williams, and C. E. Dempsey. 1997. Helix bending in alamethicin: molecular dynamics simulations and amide hydrogen exchange in methanol. *Biophys. J.* 72:2490–2495.

Goormaghtigh, E., V. Raussens, and J. Ruysschaert. 1999. Attenuated total reflection infrared spectroscopy of proteins and lipids in biological membranes. *Biochim. Biophys. Acta.* 1422:105–115.

Halsall, A., and C. E. Dempsey. 1999. Intrinsic helical propensities and stable secondary structure in a membrane-bound fragment (s4) of the Shaker potassium channel. *J. Mol. Biol.* 293:901–915.

He, K., S. Ludtke, W. Heller, and H. Huang. 1996. Mechanism of alamethicin insertion into lipid bilayers. *Biophys. J.* 71:2669–2679.

Heller, W. T., K. He, S. J. Ludtke, T. A. Harroun, and H. W. Huang. 1997. Effect of changing the size of lipid headgroup on peptide insertion into membranes. *Biophys. J.* 73:239–244.

Helluin, O., J. Y. Dugast, G. Molle, A. R. Mackie, S. Ladha, and H. Duclohier. 1997. Lateral diffusion and conductance properties of a fluorescein-labelled alamethicin in planar lipid bilayers. *Biochim. Biophys. Acta.* 1330:284–292.

Hess, B., H. Bekker, H. J. C. Berendsen, and J. G. E. M. Fraaije. 1997. LINCS: A linear constraint solver for molecular simulations. *J. Comp. Chem.* 18:1463–1472.

Hille, B. 1992. Ionic Channels of Excitable Membranes. 2d edition. Sinauer Associates, Inc., Sunderland, MA.

Hol, W. G. J. 1985. The role of the alpha-helix dipole in protein function and structure. *Prog. Biophys. Mol. Biol.* 45:149–195.

Hristova, K., W. C. Wimley, V. K. Mishra, G. Anantharamiah, J. P. Segrest, and S. H. White. 1999. An amphipathic alpha-helix at a membrane interface: a structural study using a novel X-ray diffraction method. *J. Mol. Biol.* 290:99–117.

Huang, H. W., and Y. Wu. 1991. Lipid-alamethicin interactions influence alamethicin orientation. *Biophys. J.* 60:1079–1087.

Hunenberger, P. H., and J. A. McCammon. 1999. Effect of artificial periodicity in simulations of biomolecules under Ewald boundary conditions: a continuum electrostatics study. *Biophys. Chem.* 78:69–88.

Jayasinghe, S., M. Barranger-Mathys, J. Ellena, C. Franklin, and D. Cafiso. 1998. Structural features that modulate the transmembrane migration of a hydrophobic peptide in lipid vesicles. *Biophys. J.* 74:3023–3030.

Kabsch, W., and C. Sander. 1983. Dictionary of protein secondary structure: Pattern recognition of hydrogen-bonded and geometrical features. *Biopolymers.* 22:2577–2637.

Kessel, A., D. S. Cafiso, and N. Ben-Tal. 2000. Continuum solvent model calculations of alamethicin-membrane interactions: thermodynamic aspects. *Biophys. J.* 78:571–583.

Korzhnev, D. M., V. Y. Orekhov, A. S. Arseniev, R. Gratias, and H. Kessler. 1999. Mechanism of the unfolding of transmembrane alpha-helical segment (1–36)-bacteriorhodopsin studied by molecular dynamics simulations. *J. Phys. Chem. B.* 103:7036–7043.

Kovacs, F. A., J. K. Denny, Z. Song, J. R. Quine, and T. A. Cross. 2000. Helix tilt of the M2 transmembrane peptide from influenza a virus: An intrinsic property. *J. Mol. Biol.* 295:117–125.

Kraulis, P. J. 1991. MOLSCRIPT: a program to produce both detailed and schematic plots of protein structures. *J. Appl. Crystallogr.* 24:946–950.

Kukol, A., P. Adams, L. Rice, A. Brunger, and I. Arkin. 1999. Experimentally based orientational refinement of membrane protein models: A structure for the Influenza A M2 H+ channel. *J. Mol. Biol.* 286:951–962.

La Rocca, P., P. Biggin, D. P. Tieleman, and M. S. P. Sansom. 1999. Simulation studies of the interaction of antimicrobial peptides and lipid bilayers. *Biochim. Biophys. Acta.* 1462:185–200.

Ladokhin, A. S., and S. H. White. 1999. Folding of amphipathic alpha-helices on membranes: energetics of helix formation by melittin. *J. Mol. Biol.* 285:1363–1369.

Lewis, J. R., and D. S. Cafiso. 1999. Membrane spontaneous curvature modulates the binding energy of a channel forming voltage-gated peptide. *Biochemistry.* 38:5932–5938.

Lu, L., and C. Deber. 1998. Guidelines for membrane protein engineering derived from de novo designed model peptides. *Biopolymers.* 47:41–62.

Marassi, F. M., and S. J. Opella. 1998. NMR structural studies of membrane proteins. *Curr. Opin. Struct. Biol.* 8:640–648.

Miyazawa, A., Y. Fujiyoshi, M. Stowell, and N. Unwin. 1999. Nicotinic acetylcholine receptor at 4.6 angstrom resolution: Transverse tunnels in the channel wall. *J. Mol. Biol.* 288:765–786.

North, C. L., M. Barranger-Mathys, and D. S. Cafiso. 1995. Membrane orientation of the N-terminal segment of alamethicin determined by solid-state ^{15}N NMR. *Biophys. J.* 69:2392–2397.

Roux, B. 1997. Influence of the membrane potential on the free energy of an intrinsic protein. *Biophys. J.* 73:2980–2989.

Sansom, M. S. P. 1991. The biophysics of peptide models of ion channels. *Prog. Biophys. Mol. Biol.* 55:139–236.

Sansom, M. S. P. 1993. Structure and function of channel-forming peptaibols. *Quart. Rev. Biophys.* 26:365–421.

Sansom, M. S. P. 2000. Potassium channels: watching a voltage-sensor tilt and twist. *Curr. Biol.* 10:R206–R209.

Sansom, M. S. P., D. P. Tieleman, and H. J. C. Berendsen. 1999. The mechanism of channel formation by alamethicin as viewed by molecular dynamics simulations. *Novartis Foundation Symp.* 225:128–141.

Schuler, L. D., and W. F. van Gunsteren. 2000. On the choice of dihedral angle potential functions for n-alkanes. *Mol. Sim.* (in press)

Smith, P., and W. F. van Gunsteren. 1994. Consistent dielectric-properties of the simple point-charge and extended simple point-charge water models at 277 and 300 K. *J. Chem. Phys.* 100:3169–3174.

Stryer, L. 1988. Biochemistry. 3d edition. W.H. Freeman and Company, New York.

Tieleman, D. P., H. J. C. Berendsen, and M. S. P. Sansom. 1999a. An alamethicin channel in a lipid bilayer: molecular dynamics simulations. *Biophys. J.* 76:1757–1769.

Tieleman, D. P., H. J. C. Berendsen, and M. S. P. Sansom. 1999b. Surface binding of alamethicin stabilises its helical structure: molecular dynamics simulations. *Biophys. J.* 76:3186–3191.

Tieleman, D. P., S. J. Marrink, and H. J. C. Berendsen. 1997. A computer perspective of membranes: molecular dynamics studies of lipid bilayer systems. *Biochim. Biophys. Acta.* 1331:235–270.

Tieleman, D. P., M. S. P. Sansom, and H. J. C. Berendsen. 1999c. Alamethicin helices in a bilayer and in solution: Molecular dynamics simulations. *Biophys. J.* 76:40–49.

van der Spoel, D., A. R. van Buuren, E. Apol, P. J. Meulenhoff, D. P. Tieleman, A. L. T. M. Sijbers, B. Hess, K. A. Feenstra, R. van Drunen, and H. J. C. Berendsen. 1998. Gromacs User Manual version 2.0. Nijenborgh 4, 9747 AG Groningen, The Netherlands. (Internet: http://rugmd.chem.rug.nl/~gmx)

van Gunsteren, W. F., P. Krüger, S. R. Billeter, A. E. Mark, A. A. Eising, W. R. P. Scott, P. H. Hüneberger, and I. G. Tironi. 1996. Biomolecular Simulation: The GROMOS96 Manual and User Guide. Biomos/Hochschulverlag AG an der ETH Zürich, Groningen/Zürich.

Vogel, H. 1987. Comparison of the conformation and orientation of alamethicin and melittin in lipid membranes. *Biochemistry.* 26:4562–4572.

White, S. H., and W. C. Wimley. 1998. Hydrophobic interactions of peptides with membrane interfaces. *Biochim. Biophys. Acta.* 1376:339–352.

White, S. H., and W. C. Wimley. 1999. Membrane protein folding and stability: physical principles. *Annu. Rev. Biophys. Biomol. Struct.* 28: 319–365.

Wieprecht, T., O. Apostolov, M. Beyermann, and J. Seelig. 1999. Thermodynamics of the alpha-helix-coil transition of amphipathic peptides in a membrane environment: Implications for the peptide-membrane binding equilibrium. *J. Mol. Biol.* 294:785–794.

Woolley, G. A., P. C. Biggin, A. Schultz, L. Lien, D. C. J. Jaikaran, J. Breed, K. Crowhurst, and M. S. P. Sansom. 1997. Intrinsic rectification of ion flux in alamethicin channels: Studies with an alamethicin dimer. *Biophys. J.* 73:770–778.

Woolley, G. A., and B. A. Wallace. 1992. Model ion channels: gramicidin and alamethicin. *J. Membr. Biol.* 129:109–136.

Wu, Y., K. He, S. J. Ludtke, and H. W. Huang. 1995. X-ray diffraction study of lipid bilayer membrane interacting with amphiphilic helical peptides: diphytanoyl phosphatidylcholine with alamethicin at low concentrations. *Biophys. J.* 68:2361–2369.

Zhou, F. X., M. J. Cocco, W. P. Russ, A. T. Brunger, and D. M. Engelman. 2000. Interhelical hydrogen bonding drives strong interactions in membrane proteins. *Nat. Struct. Biol.* 7:154–160.